Voltammetric, Specular Reflectance Infrared, and X-ray Electron Probe Characterization of Redox and Isomerization Processes Associated with the $[Mn(CO)_2(\eta^3\text{-}P_2P')Br]^{+/0}$ ($P_2P' = \{Ph_2P(CH_2)_2\}_2PPh$), $[Mn(CO)_2(\eta^3\text{-}P_3P')Br]^{+/0}$ ($P_3P' = \{Ph_2PCH_2\}_3P$), and $[\{Mn(CO)_2(\eta^2\text{-dpe})Br\}_2(\mu\text{-dpe})]^{2+/0}$ (dpe = $Ph_2P(CH_2)_2PPh_2$) Solid State Systems

Alan M. Bond,*,[1] Ray Colton,[1] Frank Marken,[2] and Jacky N. Walter[3]

Department of Chemistry, Monash University, Clayton, Victoria 3168, Australia, Physical and Theoretical Chemistry Laboratory, Oxford University, South Parks Road, Oxford OX1 3QZ, U.K., and School of Chemistry, La Trobe University, Bundoora, Victoria 3083, Australia

Received June 5, 1997[⊗]

Extremely well defined voltammetric responses are obtained for both oxidation of microcrystalline mononuclear *trans*- and *cis,mer*-$Mn(CO)_2(\eta^3\text{-}P_2P')Br$ ($P_2P' = \{Ph_2P(CH_2)_2\}_2$-PPh) and *cis,mer*-$Mn(CO)_2(\eta^3\text{-}P_3P')Br$ ($P_3P' = \{Ph_2PCH_2\}_3P$) and binuclear *cis,fac*-$\{Mn(CO)_2$-$(\eta^2\text{-dpe})Br\}_2(\mu\text{-dpe})$ (dpe = $Ph_2P(CH_2)_2PPh_2$) and reduction of cationic *trans*-$[Mn(CO)_2(\eta^3$-$P_2P')Br]BF_4$, *trans*-$[Mn(CO)_2(\eta^3\text{-}P_3P')Br]BF_4$, and *trans*-$[\{Mn(CO)_2(\eta^2\text{-dpe})Br\}_2(\mu\text{-dpe})](BF_4)_2$ when they are attached to a graphite electrode and placed in water containing either 0.1 M NaCl or KCl as the electrolyte. The combination of access to species in different oxidation states and different isomeric forms, as well as mononuclear and binuclear species, enables the rates of isomerization and the extent of electronic communication between the metal centers to be evaluated in the solid state and compared to data in organic solvent systems previously reported. The voltammetric data, combined with specular reflectance IR and X-ray electron probe data, established that the following processes occur at the graphite electrode−microcrystal−water (electrolyte) interface (subscript "s" denotes solid): *trans*-$Mn(CO)_2(\eta^3\text{-}P_2P')Br_s + Cl^- \rightleftharpoons$ *trans*-$[Mn(CO)_2(\eta^3\text{-}P_2P')Br]Cl_s + e^-$; *cis,mer*-$Mn(CO)_2(\eta^3\text{-}P_2P')$-$Br_s + Cl^- \rightleftharpoons$ *cis,mer*-$[Mn(CO)_2(\eta^3\text{-}P_2P')Br]Cl_s + e^- \rightarrow$ *trans*-$[Mn(CO)_2(\eta^3\text{-}P_2P')Br]Cl_s$; *trans*-$Mn(CO)_2(\eta^3\text{-}P_3P')Br_s + Cl^- \rightleftharpoons$ *trans*-$[Mn(CO)_2(\eta^3\text{-}P_3P')Br]Cl_s + e^-$; *cis,mer*-$Mn(CO)_2(\eta^3\text{-}P_3P')Br_s$ $+ Cl^- \rightleftharpoons$ *cis,mer*-$[Mn(CO)_2(\eta^3\text{-}P_3P')Br]Cl_s + e^- \rightarrow$ *trans*-$[Mn(CO)_2(\eta^3\text{-}P_3P')Br]Cl_s$; *trans*-$\{Mn$-$(CO)_2(\eta^2\text{-dpe})Br\}_2(\mu\text{-dpe})_s + 2Cl^- \rightleftharpoons$ *trans*-$[\{Mn(CO)_2(\eta^2\text{-dpe})Br\}_2(\mu\text{-dpe})]Cl_{2\ s} + 2e^-$; *cis,fac*-$\{Mn(CO)_2(\eta^2\text{-dpe})Br\}_2(\mu\text{-dpe})_s + 2Cl^- \rightleftharpoons$ *cis,fac*-$[\{Mn(CO)_2(\eta^2\text{-dpe})Br\}_2(\mu\text{-dpe})]Cl_{2\ s} + 2e^- \rightarrow$ *trans*-$[\{Mn(CO)_2(\eta^2\text{-dpe})Br\}_2(\mu\text{-dpe})]Cl_{2\ s}$. The reaction pathways in organic solvents are generally analogous. However, the rates of isomerization are slower in the solid state, and shapes of voltammograms and potentials differ significantly. Interestingly, in the binuclear $[\{Mn(CO)_2(\eta^2\text{-dpe})Br\}_2(\mu\text{-dpe})]^{2+/0}$ system, no intermediate $[\{Mn(CO)_2(\eta^2\text{-dpe})Br\}_2(\mu\text{-dpe})]^+$ species are observed in the solid state, implying that the metal centers are oxidized or reduced at the same potentials, unlike the case in the solution phase, where the $[\{Mn(CO)_2(\eta^2\text{-dpe})$-$Br\}_2(\mu\text{-dpe})]^{2+/+}$ and $[\{Mn(CO)_2(\eta^2\text{-dpe})Br\}_2(\mu\text{-dpe})]^{+/0}$ redox couples are well separated. This result implies that no significant communication occurs between the metal centers in the solid state redox processes.

Introduction

Electrochemical studies on redox-active nonconducting inorganic and organometallic compounds are rare. However, recently it has been shown[4] that voltammetric studies on nonconducting solids are possible, provided they are attached to an electrode as well-spaced microcrystals (size < 10 μm). For example, the microcrystals may be mechanically attached to graphite electrodes which are then placed in a solvent (electrolyte) medium in which the compound is insoluble. The redox processes can then take place at the electrode−microcrystal−solvent (electrolyte) boundary, with charge neutralization achieved, if necessary, via transport of the appropriate electrolyte ion present in the solution to the crystal or from the crystal to the solvent.

In the present study, this new technique for studying the redox properties of organometallic solids has been applied to oxidation of microcrystals of neutral *cis,mer*- and *trans*-$Mn(CO)_2(\eta^3\text{-}P_2P')Br$ ($P_2P' = \{Ph_2P(CH_2)_2\}_2$-

⊗ Abstract published in *Advance ACS Abstracts,* October 1, 1997.
(1) Monash University.
(2) Oxford University.
(3) La Trobe University.
(4) (a) Scholz, F.; Lange, B. *Trends Anal. Chem.* **1992**, *11*, 359. (b) Scholz, F.; Meyer, B. *Chem. Soc. Rev.* **1994**, *23*, 341. (c) Bond, A. M.; Colton, R.; Daniels, F.; Fernando, D. R.; Marken, F.; Nagaosa, Y.; Van Stevenick, R. F. M.; Walter, J. N. *J. Am. Chem. Soc.* **1993**, *115*, 9556. (d) Bond, A. M.; Colton, R.; Marken, F.; Walter, J. N. *Organometallics* **1994**, *13*, 5122. (e) Bond, A. M.; Marken, F. *J. Electroanal. Chem. Interfacial Electrochem.* **1994**, *372*, 125.

S0276-7333(97)00468-8 CCC: $14.00

PPh) and the analogous $Mn(CO)_2(\eta^3\text{-}P_3P')Br$ compounds ($P_3P' = \{Ph_2PCH_2\}_3P$), together with *cis,fac*-$\{Mn(CO)_2(\eta^2\text{-dpe})Br\}_2(\mu\text{-dpe})$ (dpe = $Ph_2P(CH_2)_2PPh_2$), and the reduction of *trans*-$[Mn(CO)_2(\eta^3\text{-}P_2P')Br]BF_4$, *trans*-$[Mn(CO)_2(\eta^3\text{-}P_3P')Br]BF_4$, and *trans*-$[\{Mn(CO)_2(\eta^2\text{-dpe})Br\}_2(\mu\text{-dpe})](BF_4)_2$. This series of compounds was chosen to include examples of mononuclear and binuclear systems where isomerizations in the solid state can occur. Additionally, since the binuclear complexes have two metal centers which can be oxidized, the separation of potential for their oxidation provides information on the extent of communication between the metal centers in the solid state.

In order to make the required measurements, the crystals were mechanically attached to graphite electrodes which were then placed in water containing 0.1 M NaCl or KCl as the electrolyte. The redox reaction of the water-insoluble compound was then monitored by voltammetry, specular reflectance IR spectroscopy, and also X-ray electron probe techniques. Access to both oxidation states of mononuclear $[Mn(CO)_2(\eta^3\text{-}P_2P')Br]^{+/0}$ and $[Mn(CO)_2(\eta^3\text{-}P_3P')Br]^{+/0}$ and the binuclear $[\{Mn(CO)_2(\eta^2\text{-dpe})Br\}_2(\mu\text{-dpe})]^{2+/0}$ systems enables detailed voltammetric studies to be undertaken in both the oxidation and reduction directions, while the IR measurements enable stereochemical changes (geometrical isomerizations) to be detected. The X-ray electron probe method enables detection of K^+ or Cl^-, if these ions are incorporated into the structures as part of the charge neutralization process.

Finally, it is of considerable interest to compare results with solution phase voltammetric studies which have been conducted in dichloromethane (0.1 M Bu_4NPF_6),[5−7] since intuitively it might be expected that isomerization rates and communication between the metal centers would be significantly different in solid and solution phases.

Experimental Section

Synthesis. The compounds *cis,mer*-$Mn(CO)_2(\eta^3\text{-}P_2P')Br$ and *trans*-$[Mn(CO)_2(\eta^3\text{-}P_2P')Br]BF_4$,[5] the analogous $\eta^3\text{-}P_3P'$ complexes,[6] and the binuclear species *cis,fac*-$\{Mn(CO)_2(\eta^2\text{-dpe})Br\}_2(\mu\text{-dpe})$[7] were prepared as described previously by interaction of $Mn(CO)_5Br$ with the appropriate ligand. *trans*-$[\{Mn(CO)_2(\eta^2\text{-dpe})Br\}_2(\mu\text{-dpe})](BF_4)_2$ has previously been characterized in solution,[7] and it was isolated by oxidizing *cis,fac*-$\{Mn(CO)_2(\eta^2\text{-dpe})Br\}_2(\mu\text{-dpe})$ with $NOBF_4$ in dichloromethane solution at room temperature, removing the solvent under vacuum, and recrystallizing the resulting solid from dichloromethane/hexane.

Reagents and Voltammetric Instrumentation. All reagents were of analytical or electrochemical grade purity. Water from a Millipore system was used for the preparation of aqueous electrolyte solution. The reference electrode used was a Ag/AgCl (3 M NaCl) electrode, and the auxiliary electrode was made from a platinum sheet. Voltammetric experiments were performed with a BAS 100 A electrochemical analyzer (Bioanalytical Systems, West Lafayette, IN). All solutions were deaerated with high-purity nitrogen for 15 min prior to making the measurements.

The carbon disk electrodes were made from basal plane pyrolytic graphite (5 mm diameter) fitted into a Teflon holder. Solids (1−3 mg) were placed on a coarse grade filter paper, and the electrode was pressed onto the solid and rubbed over the material, so some adhered to the electrode surface as an array of microcrystalline particles of 0.1−10 μm size. For electrochemical measurements, the electrode was transferred into the electrochemical cell containing aqueous electrolyte solution. The electrode surface could be renewed after measurements by dissolving the solid with dichloromethane.

Specular Reflectance FT-IR Spectroscopy. The electrode surface with adhered solid exhibits a shiny surface which is an excellent reflector of light. A specular reflectance system (angle of incidence 30°) mounted in a Perkin-Elmer FT-IR 1720 spectrometer gave strong and reproducible signals, which correspond closely with absorption bands observed in solution spectra. Electrodes were rinsed in water after electrochemical experiments and dried in air before spectra were acquired. Typically, 10−20 scans were sufficient when good background subtraction could be achieved.

X-ray Electron Probe Analysis. Surface elemental analyses by electron probe X-ray measurements were carried out on a scanning electron microscope (JSM 840) coupled to a TN 5500 X-ray analyzer at an accelerating voltage of 15 kV, with a probe monitor current ranging from 0.3 to 0.6 nA. A dead time of 25−30% is present under these conditions for a spectrum collection time of 100 s. Samples for analysis were prepared by rubbing a freshly cleaved basal plane carbon graphite plate (5 mm × 5 mm × 1 mm) onto a small amount of the carbonyl compound on filter paper. After electrolysis at the required potential for 120 s in the aqueous (electrolyte) solution, the plate was transferred to a bath of distilled water and then dried in air. The carbon plates were attached to the sample holder with conducting epoxy resin.

Scanning Electron Microscopy. An ETEC Autoscan system (20 kV accelerator voltage) was used for scanning electron microscopy measurements. Sample preparation was similar to that described for the electron probe analyzer. The surface-modified carbon plate was fixed with double-sided tape on a stub and gold-plated in a Balzers sputter-coating unit.

Results and Discussion

***trans*- and *cis,mer*-$Mn(CO)_2(\eta^3\text{-}P_2P')Br$ and *trans*-$[Mn(CO)_2(\eta^3\text{-}P_2P')Br]BF_4$. (a) Electrochemical Studies.** Except for the fact that peak current magnitudes varied according to the amount of solid on the graphite electrode surface, voltammograms showed similar characteristics for all experiments. The electrochemical data are summarized in Table 1, and peak potentials are referenced against Ag/AgCl (3 M NaCl). The geometries of the compounds are shown in structures **I** and **II**.

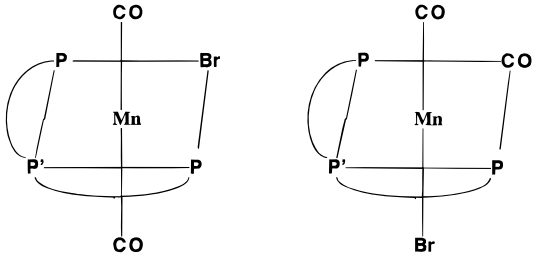

trans-$Mn(CO)_2(\eta^3\text{-}P_2P')Br$ **(I)** *cis,mer*-$Mn(CO)_2(\eta^3\text{-}P_2P')Br$ **(II)**

A cyclic voltammogram (scan rate, 200 mV s^{-1}) for the oxidation of *trans*-$Mn(CO)_2(\eta^3\text{-}P_2P')Br$ mechanically attached to a graphite electrode and immersed in aqueous solution (0.1 M NaCl) at 20 °C (Figure 1a) shows an oxidation response at 0.46 V. This process corresponds to that observed in solution,[5] except that Cl^- ions are incorporated into the solid to achieve charge neutrality (see X-ray electron probe data later), and is

(5) Bond, A. M.; Colton, R.; Walter, J. N. *Inorg. Chem.* **1997,** *36,* 1181.
(6) Bond, A. M.; Colton, R.; Walter, J. N. *Inorg. Chem.*, submitted for publication.
(7) Bond, A. M.; Colton, R.; Walter, J. N. *Inorg. Chem.*, submitted for publication.

Table 1. Voltammetric Data (Scan Rate, 200 mV s^{-1}) for Solid *trans*- and *cis,mer*-$Mn(CO)_2(\eta^3\text{-}P_2P')Br$ and *trans*-$[Mn(CO)_2(\eta^3\text{-}P_2P')Br]BF_4$ Mechanically Attached to Graphite Electrodes and Placed in Aqueous Solution (0.1 M NaCl)[a]

		potential (V vs Ag/AgCl)			ΔE_p	temp
compound	process	E_p^{ox}	E_p^{red}	$E^r_{1/2}$	(mV)	(°C)
trans[0 b]	1a,a′	0.46	0.08	0.27	380	20
	1a,a′	0.42	0.10	0.26	320	30
	1a,b′	0.42	0.16	0.19	260	30
	1a,b′	0.41	0.17	0.29	240	40
	1a,b′	0.36	0.20	0.28	160	50
trans[0 c]	1a,a′	0.34	0.06	0.20	280	20
	1a,a′	0.32	0.08	0.20	240	30
	1a,a′	0.32	0.09	0.21	230	40
	1a,b′	0.32	0.16	0.24	160	40
	1a,a′	0.31	0.11	0.21	200	50
	1a,b′	0.31	0.20	0.26	110	50
trans[+ b]	1a,a′	0.29	0.10	0.20	190	20
	1a,b′	0.29	0.17	0.23	120	30
	1a,b′	0.29	0.19	0.24	100	40
	1a,a′	0.29	0.11	0.20	180	50
	1a,b′	0.29	0.20	0.25	90	50
trans[+ c]	1a,a′	0.29	0.06	0.18	230	20
	1a,a′	0.29	0.06	0.18	230	30
	1a,b′	0.29	0.16	0.23	130	30
	1a,a′	0.30	0.07	0.19	230	40
	1a,b′	0.30	0.18	0.24	120	40
	1a,a′	0.30	0.10	0.20	200	50
	1a,b′	0.30	0.19	0.25	110	50
cis,mer[0 d]	1a,a′	0.31	0.11	0.21	200	50
	2	0.73	0.61	0.67	120	50
	3	0.81	0.72	0.77	90	50

[a] E_p^{ox}, oxidation peak potential; E_p^{red}, reduction peak potential; $E^r_{1/2}$, reversible redox potential; ΔE_p, peak separation. [b] Potentials for first scan. [c] Potentials after several scans. [d] Potentials are given for second scan as initial oxidation response for process 3 merges with the background for first scan.

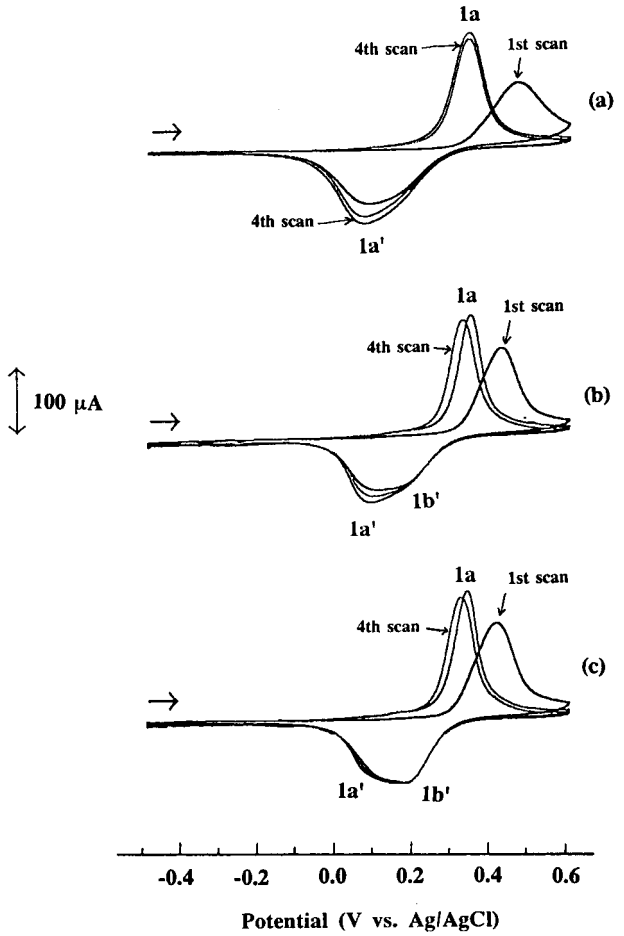

Figure 1. Cyclic voltammograms (first, second, and fourth scans; scan rate, 200 mV s^{-1}) of solid *trans*-$Mn(CO)_2(\eta^3\text{-}P_2P')Br$ mechanically attached to graphite electrodes and placed in aqueous solution (0.1 M NaCl) at (a) 20, (b) 30, and (c) 40 °C.

shown in eq 1, where the subscript "s" indicates a solid compound. The reverse scan reveals a reduction re-

$$\textit{trans}\text{-}Mn(CO)_2(\eta^3\text{-}P_2P')Br_s + Cl^- \rightleftharpoons \textit{trans}\text{-}[Mn(CO)_2(\eta^3\text{-}P_2P')Br]Cl_s + e^- \quad (1)$$

sponse at 0.08 V, assigned as process 1a′ to differentiate this response from another reduction wave which is present at higher temperatures (in this paper, all reduction responses will be denoted by a prime). The second cycle contains a sharper oxidation wave (process 1a) which has a greater peak height and occurs at a significantly less positive potential than the oxidation response of the first cycle. The reduction response also shows enhanced peak current on the second cycle but is observed at almost the same potential as on the first cycle. Subsequent cycles show little variation from the second cycle. The difference between the first and second cycles has been noted previously.[4b] Presumably, interaction between the compound and the solvent during the course of redox recycling produces changes in the size, shape, and structure of the crystals, which are most pronounced in the initial stages of the voltammetric experiments.

Cyclic voltammograms were recorded at higher temperatures, after cleaning the graphite electrode and attaching fresh *trans*-$Mn(CO)_2(\eta^3\text{-}P_2P')Br$ for each temperature. At 30 °C (Figure 1b), another reduction response (process 1b′) is clearly observed when the scan direction is reversed. Only one oxidation wave is apparent upon repetitive cycling of the potential, while process 1a′ gradually becomes the dominant reduction response. A cyclic voltammogram obtained at 40 °C (Figure 1c) indicates that process 1b′ is much more prominent than process 1a′ on the first cycle, but repetitive cycling of the potential shows the gradual growth of process 1a′. At 50 °C, process 1b′ is the dominant reduction process, while process 1a′ is barely observed on the first cycle but becomes more obvious after several cycles. As the temperature is increased, the potential difference between the oxidation response on the first and successive scans decreases, as does the peak-to-peak separations (ΔE_p) for processes 1a,a′ and 1a,b′. Peak splittings, such as that observed for this system, have been reported for other complexes[4b,c] which for the *trans*-$[Mn(CO)_2(\eta^3\text{-}P_2P')Br]^{+/0}$ system are attributed to formation of different phases rather than new species. IR data given below support this conclusion.

A reductive cyclic voltammogram (scan rate, 200 mV s^{-1}) of solid *trans*-$[Mn(CO)_2(\eta^3\text{-}P_2P')Br]BF_4$ attached to a graphite electrode and recorded at 20 °C (Figure 2a) shows on the first cycle only a single reduction process (process 1a′) and a single oxidation wave (process 1a). Subsequent cycles show a small shift toward a less positive potential for the reduction process 1a′, while the oxidation response appears virtually unaltered. This contrasts with the voltammograms for the oxidation of

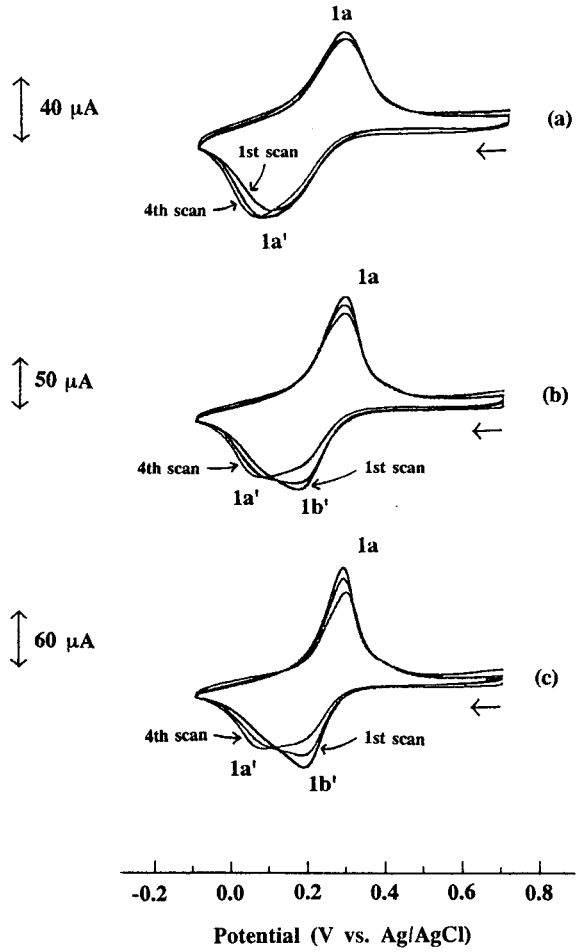

Figure 2. Cyclic voltammograms (first, second, and fourth scans; scan rate, 200 mV s^{-1}) of solid *trans*-[$Mn(CO)_2(\eta^3$-$P_2P')Br]BF_4$ mechanically attached to graphite electrodes and placed in aqueous solution (0.1 M NaCl) at (a) 20, (b) 30, and (c) 40 °C.

trans-$Mn(CO)_2(\eta^3$-$P_2P')Br$, where the shape and position of this process vary considerably between the first and second cycles. A cyclic voltammogram obtained at 30 °C is shown in Figure 2b. At this temperature, the first reductive scan indicates that process 1b′ is the dominant reduction process, but again, repetitive cycling shows the growth of reduction process 1a′ while process 1b′ diminishes. Thus, regardless of whether the initial complex is *trans*-$Mn(CO)_2(\eta^3$-$P_2P')Br$ or *trans*-[$Mn(CO)_2$-$(\eta^3$-$P_2P')Br]BF_4$, process 1a′ is the dominant reduction process observed after several scans. At 40 °C (Figure 2c) and at 50 °C, the results obtained for *trans*-[Mn-$(CO)_2(\eta^3$-$P_2P')Br]BF_4$ are analogous to those observed for *trans*-$Mn(CO)_2(\eta^3$-$P_2P')Br$.

Figure 3a shows a cyclic voltammogram recorded at 50 °C for the oxidation of solid *cis,mer*-$Mn(CO)_2(\eta^3$-$P_2P')$-Br attached to a graphite electrode. On the first cycle, an oxidation response is barely resolved from the solvent background, while several reduction waves are observed on the reverse scan. A second cycle clearly shows the presence of two oxidation responses (processes 2 and 3) which are very close together. Reduction responses (processes 2′ and 3′) corresponding to these oxidation waves are apparent, together with an additional reduction response (process 1a′) at a less positive potential. When the potential range is restricted slightly and several more cycles are recorded (Figure 3b), three redox couples are apparent corresponding to couples 2, 3, and

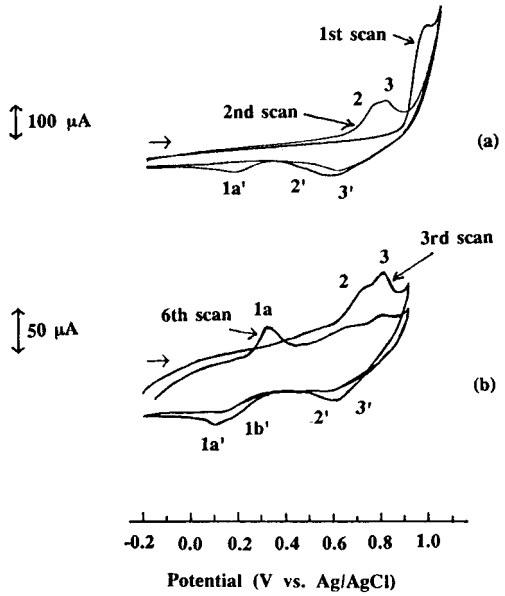

Figure 3. Cyclic voltammograms (scan rate, 200 mV s^{-1}) at 50 °C of solid *cis,mer*-$Mn(CO)_2(\eta^3$-$P_2P')Br$ mechanically attached to a graphite electrode and placed in aqueous solution (0.1 M NaCl). (a) first and second scans; (b) third and sixth scans.

1 (the *cis,mer*$^{+/0}$, *cis,fac*$^{+/0}$, and *trans*$^{+/0}$ redox couples, respectively) which were observed in dichloromethane and acetone solutions.[5] Process 1b′ now also is present. The current associated with processes 2 and 3 decreases with successive scans, while processes 1a and 1a′ increase until eventually processes 2 and 3 are no longer observed. The peak potentials are similar to those obtained with either *trans*-$Mn(CO)_2(\eta^3$-$P_2P')Br$ or *trans*-[$Mn(CO)_2(\eta^3$-$P_2P')Br]BF_4$ at 50 °C after several scans. Thus, isomerization from the 17-electron *cis,mer*$^+$ to the *cis,fac*$^+$ and *trans*$^+$ geometries occurs in both solution and solid state phases, and the overall mechanism for the oxidation of solid *cis,mer*-$Mn(CO)_2(\eta^3$-$P_2P')Br$ is

$$cis,mer\text{-}Mn(CO)_2(\eta^3\text{-}P_2P')Br_s + Cl^- \rightleftharpoons cis,mer\text{-}[Mn(CO)_2(\eta^3\text{-}P_2P')Br]Cl_s + e^- \xrightarrow{\text{slow}} trans\text{-}[Mn(CO)_2(\eta^3\text{-}P_2P')Br]Cl_s \quad (2)$$

In acetone solution at 50 °C, processes 2 and 3 merge because of fast isomerization between the *cis,mer*$^+$ and *cis,fac*$^+$ geometries,[5] but the individual redox couples are apparent at 20 °C, where the isomerization rate is slower. The above data suggest that the isomerization reactions are slower for the surface-confined species. Similar observations were made for the oxidation of *cis*-$Cr(CO)_2(\eta^2$-dpe$)_2$, for which the rate of isomerization from *cis*$^+$ to *trans*$^+$ species appears faster in solution than in the solid state.[4b]

(b) IR Spectroscopy. Specular reflectance FT-IR spectroscopy was used to characterize the redox chemistry of the solid materials attached to the graphite electrode. The IR spectrum of solid *trans*-$Mn(CO)_2(\eta^3$-$P_2P')Br$ attached to a graphite electrode (Figure 4a) shows a single carbonyl stretch at 1901 cm^{-1}, a slightly higher frequency than that for the corresponding band observed in dichloromethane solution (1893 cm^{-1}). When oxidation of the solid is undertaken at 0.400 V for 10 s, an additional carbonyl IR band is observed at

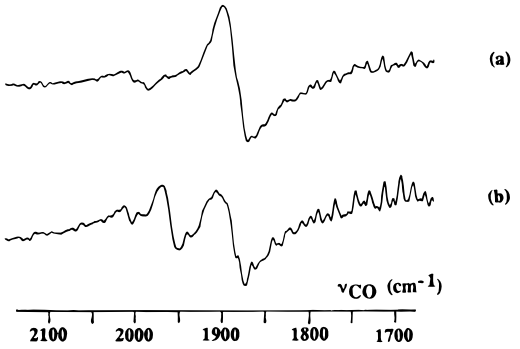

Figure 4. Specular reflectance FT-IR spectra (20 °C) obtained for *trans*-[Mn(CO)$_2$(η^3-P$_2$P′)Br mechanically attached to a graphite electrode (a) before oxidation and (b) after oxidation at 0.400 V for 10 s in aqueous solution (0.1 M NaCl) at 50 °C.

Table 2. IR Data (20 °C) for the Solid Compounds Mechanically Attached to Graphite Electrodes

compound	ν_{CO} (cm^{-1})
cis,mer-Mn(CO)$_2$(η^3-P$_2$P′)Br	1937, 1862
trans-Mn(CO)$_2$(η^3-P$_2$P′)Br	1901
trans-[Mn(CO)$_2$(η^3-P$_2$P′)Br]BF$_4$	1967
cis,mer-Mn(CO)$_2$(η^3-P$_3$P′)Br	1940, 1861
trans-Mn(CO)$_2$(η^3-P$_3$P′)Br	1899
trans-[Mn(CO)$_2$(η^3-P$_3$P′)Br]BF$_4$	1966
cis,fac-{Mn(CO)$_2$(η^2-dpe)Br}$_2$(μ-dpe)	1937, 1865
trans-[{Mn(CO)$_2$(η^2-dpe)Br}$_2$(μ-dpe)](BF$_4$)$_2$	1965

1967 cm^{-1} (Figure 4b). The relative intensity of this band increases with the time of oxidation, but after approximately 1 min this band dominates the carbonyl region of the spectrum. The position of the additional band is consistent with the carbonyl stretch obtained for an isolated sample of *trans*-[Mn(CO)$_2$(η^3-P$_2$P′)Br]BF$_4$. Thus, IR spectroscopy verifies that solid *trans*-Mn(CO)$_2$-(η^3-P$_2$P′)Br is converted to *trans*-[Mn(CO)$_2$(η^3-P$_2$P′)Br]$^+$ upon oxidation. The reverse situation also applies, where *trans*-[Mn(CO)$_2$(η^3-P$_2$P′)Br]$^+$ is converted to *trans*-Mn(CO)$_2$(η^3-P$_2$P′)Br upon reduction. IR data also confirm that processes 1a′,b′ are associated with phase changes rather than formation of new species.

Solid *cis,mer*-Mn(CO)$_2$(η^3-P$_2$P′)Br attached to a graphite electrode shows two carbonyl IR bands at 1937 and 1862 cm^{-1} at positions similar to those obtained in dichloromethane solution (1936, 1866 cm^{-1}), but when the solid sample is oxidized at 0.900 V for 1 min, a carbonyl stretch becomes apparent at 1967 cm^{-1}, a position similar to that of *trans*-[Mn(CO)$_2$(η^3-P$_2$P′)Br]$^+$ in dichloromethane (1970 cm^{-1}), confirming that the initially generated *cis,mer*$^+$ isomerizes to *trans*$^+$ in the solid state. The IR data are summarized in Table 2.

(c) X-ray Electron Probe Analysis. An image produced by scanning electron microscopy of solid *cis,mer*-Mn(CO)$_2$(η^3-P$_2$P′)Br mechanically attached to a graphite plate electrode shows that a wide range of particle sizes (<1−6 μm) is present, and a significant proportion of the surface is bare graphite.

X-ray electron probe microanalysis data for a sample of solid *cis,mer*-Mn(CO)$_2$(η^3-P$_2$P′)Br attached to a graphite electrode are shown in Figure 5. Analysis of the sample before electrochemical oxidation showed the presence of Br, P, and Mn (Figure 5a). The fact that some regions of the surface did not contain these elements confirmed that much of the surface is bare graphite. Oxidation of the sample was performed at

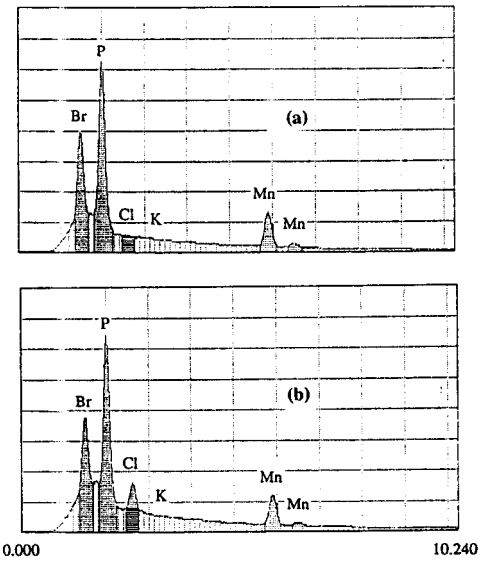

Figure 5. X-ray electron probe microanalysis data at 20 °C for solid *cis,mer*- Mn(CO)$_2$(η^3-P$_2$P′)Br mechanically attached to a graphite electrode (a) before electrolysis, showing detection of Mn, P, and Br, and (b) after oxidative electrolysis in aqueous solution (0.1 M KCl), showing detection of Mn, P, Br, and Cl, but no K.

0.900 V and 50 °C for 1 min using 0.1 M KCl as the electrolyte. KCl was used rather than NaCl as the electrolyte in this experiment since X-ray electron probe microanalysis is not very sensitive for the detection of light elements such as sodium. However, it is sensitive to the detection of potassium. Electron probe data obtained after oxidation of *cis,mer*-Mn(CO)$_2$(η^3-P$_2$P′)Br are shown in Figure 5b for a section of the surface containing particles of approximately 1 μm diameter. The presence of chloride was detected in addition to the elements mentioned above, but, importantly, no potassium was detected, indicating that the neutral aqueous KCl on the electrode surface was successfully removed by the washing process and that neither ion-paired KCl nor desolvated K$^+$ enters the crystal lattice upon oxidation of *cis,mer*-Mn(CO)$_2$(η^3-P$_2$P′)Br. Analysis of larger particles often indicated no detectable chloride or only a very small proportion of chloride, depending on which section of the particle was analyzed. Thus, the electron probe data show that oxidation of the solid does not occur uniformly across the surface of the solid but that it occurs predominantly at the edges, near the electrode−crystal−solution interface, as found for other complexes.[4b,c] Similar results were obtained when *trans*-Mn(CO)$_2$(η^3-P$_2$P′)Br was oxidized at 0.400 V or when *trans*-[Mn(CO)$_2$(η^3-P$_2$P′)Br]BF$_4$ was first reduced at 0.000 V and subsequently reoxidized at 0.400 V. Thus, the reduction step probably involves an initial ion exchange reaction,

$$\textit{trans}\text{-}[Mn(CO)_2(\eta^3\text{-}P_2P')Br][BF_4]_s + Cl^- \rightarrow \textit{trans}\text{-}[Mn(CO)_2(\eta^3\text{-}P_2P')Br]Cl_s + BF_4^- \quad (3)$$

Certainly, BF$_4^-$ is eliminated from the crystal lattice upon reduction of *trans*-[Mn(CO)$_2$(η^3-P$_2$P′)Br]BF$_4$, and Cl$^-$ becomes incorporated into the lattice upon reoxidation.

***trans*- and *cis,mer*-Mn(CO)$_2$(η^3-P$_3$P′)Br and *trans*-[Mn(CO)$_2$(η^3-P$_3$P′)Br]BF$_4$. (a) Electrochemical Stud-**

ies. The geometries of the compounds are given in structures **III** and **IV**. The first cycle of a cyclic

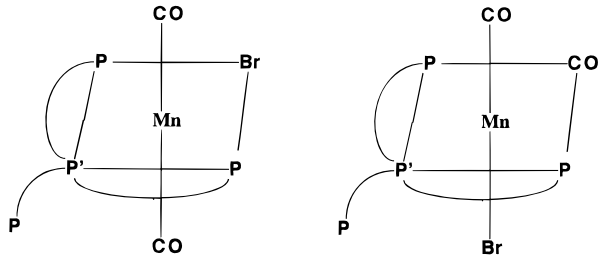

trans-Mn(CO)$_2$(η^3-P$_3$P′)Br **(III)** *cis,mer*-Mn(CO)$_2$(η^3-P$_3$P′)Br **(IV)**

voltammogram (scan rate, 200 mV s^{-1}) obtained at 20 °C for the oxidation of solid *trans*-Mn(CO)$_2$(η^3-P$_3$P′)Br attached to a graphite electrode shows an oxidation response at 0.34 V (process 1), and the corresponding reduction response (process 1′) is observed at 0.10 V on the reverse scan. Unlike the case with the *trans*-[Mn(CO)$_2$(η^3-P$_2$P′)Br]$^{+/0}$ system, no splitting of the processes occurs due to a phase change. Couple 1 is analogous to that observed in dichloromethane solution[6] and is assigned to the reaction

$$\textit{trans}\text{-Mn(CO)}_2(\eta^3\text{-P}_3\text{P}')\text{Br}_s + \text{Cl}^- \rightleftharpoons \textit{trans}\text{-[Mn(CO)}_2(\eta^3\text{-P}_3\text{P}')\text{Br]Cl}_s + \text{e}^- \quad (4)$$

with proof for chloride insertion into the solid being given later. Successive cycles indicate that the oxidation wave shifts to a less positive potential (0.28 V), although the reduction wave remains virtually unaltered. A cyclic voltammogram at 30 °C (Figure 6a) is similar to that obtained at 20° C, but at 30° C there is a smaller potential shift of the oxidation response from the first to subsequent scans. In contrast to the voltammetry at 20 and 30 °C, cyclic voltammograms obtained at 40 and 50 °C (Figure 6b) show a slight shift to a more positive potential for the second and subsequent scans compared with the first scan. At each temperature studied, the reduction response became constant after several scans.

A cyclic voltammogram (scan rate, 200 mV s^{-1}) recorded at 20 °C for the reduction of solid *trans*-[Mn(CO)$_2$(η^3-P$_3$P′)Br]BF$_4$ shows a single reduction process (process 1′), the peak potential of which appears constant over several cycles. A slight shift of the oxidation wave to a more positive potential is observed on second and subsequent cycles, and this shift is greater as the temperature is raised. A cyclic voltammogram obtained at 50 °C is shown in Figure 6c. The peak separations between oxidation and reduction waves (ΔE_p) become smaller as the temperature is raised for both *trans*-[Mn(CO)$_2$(η^3-P$_3$P′)Br]BF$_4$ and *trans*-Mn(CO)$_2$(η^3-P$_3$P′)Br, and at 50 °C after several scans, the peak potentials are identical for the two complexes, as detailed in Table 3.

Figure 7a shows the fifth and tenth cycles of a cyclic voltammogram obtained at 30 °C for the oxidation of *cis,mer*-Mn(CO)$_2$(η^3-P$_3$P′)Br. Reversible couples are observed at 0.80 (couple 3) and 0.19 V (couple 1), and a small reduction wave is apparent at 0.59 V (process 2′). An oxidation wave due to process 2 is not detected, but this response may be obscured by the oxidation wave of process 3. A similar voltammogram was obtained at 20 °C, but when the electrolyte solution is heated to 50 °C, a reduction wave corresponding to process 2′ is not

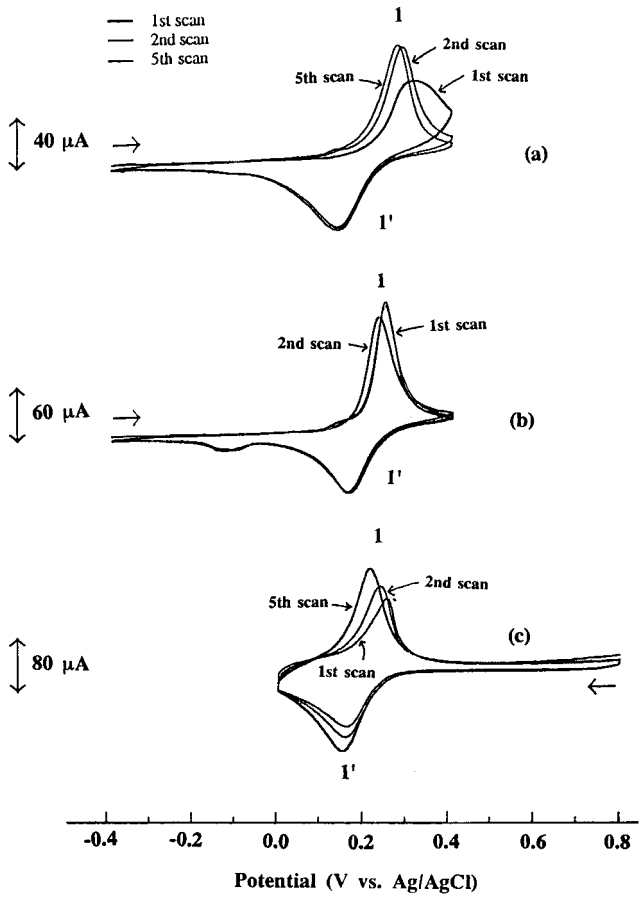

Figure 6. Cyclic voltammograms (scan rate, 200 mV s^{-1}) of solid complexes mechanically attached to graphite electrodes and placed in aqueous solution (0.1 M NaCl): (a) *trans*-Mn(CO)$_2$(η^3-P$_3$P′)Br at 30 °C, (b) *trans*-Mn(CO)$_2$-(η^3-P$_3$P′)Br at 50 °C, and (c) *trans*-[Mn(CO)$_2$(η^3-P$_3$P′)Br]BF$_4$ at 50 °C.

observed, as shown in Figure 7b. At 50 °C, the current associated with process 1 increases upon successive scans, while the current associated with the reversible couple 3 gradually decreases. The peak potentials of process 1 correlate with those of either solid *trans*-Mn(CO)$_2$(η^3-P$_3$P′)Br or *trans*-[Mn(CO)$_2$(η^3-P$_3$P′)Br]BF$_4$ after several scans at 50 °C. Thus, process 1 is assigned to the *trans*$^{+/0}$ redox couple. At lower temperatures, process 1 also becomes the dominant redox couple; however, more scans are required before this is the only redox couple present (i.e., the isomerization reactions are faster at higher temperatures).

The cyclic voltammogram at 50 °C of *cis,mer*-Mn(CO)$_2$-(η^3-P$_3$P′)Br in the solid state shows similarities to those for solutions in dichloromethane or acetone at 20 °C.[6] In the solution phase reaction, a single redox couple is observed at 20 °C and is attributed to a combination of processes 2 and 3, which involves a fast isomerization between the 17-electron *cis,mer*$^+$ and *cis,fac*$^+$ geometries. However, upon cooling of the acetone solution, the kinetics of the isomerization reactions are slowed sufficiently to enable the observation of the individual *cis,mer*$^{+/0}$ and *cis,fac*$^{+/0}$ redox couples. Thus, analogous behavior seems likely in the solid state, where at 50 °C a single redox couple is observed due to processes 2 and 3, whereas at 20 and 30 °C a small reduction wave due to process 2′ is detected. That is, the slower kinetics in the solid state relative to studies in solution mean that

Table 3. Voltammetric Data (Scan Rate, 200 mV s^{-1}) for Solid *trans*- and *cis,mer*-$Mn(CO)_2(\eta^3\text{-}P_3P')Br$ and *trans*-$[Mn(CO)_2(\eta^3\text{-}P_3P')Br]BF_4$ Mechanically Attached to Graphite Electrodes and Placed in Aqueous Solution (0.1 M NaCl)

compound	couple	potential (V vs Ag/AgCl) E_p^{ox}	E_p^{red}	$E^r_{1/2}$	ΔE_p (mV)	temp (°C)
trans$^{0\,a}$	1	0.34	0.10	0.22	230	20
	1	0.31	0.13	0.22	180	30
	1	0.25	0.15	0.20	100	40
	1	0.23	0.15	0.19	80	50
trans$^{0\,b}$	1	0.28	0.10	0.19	180	20
	1	0.27	0.13	0.20	140	30
	1	0.27	0.15	0.21	120	40
	1	0.25	0.16	0.21	90	50
trans$^{+\,a}$	1	0.24	0.08	0.16	160	20
	1	0.24	0.12	0.18	120	30
	1	0.24	0.14	0.19	100	40
	1	0.22	0.15	0.19	70	50
trans$^{+\,b}$	1	0.25	0.08	0.17	170	20
	1	0.26	0.12	0.19	140	30
	1	0.27	0.14	0.21	130	40
	1	0.25	0.16	0.21	90	50
cis,mer$^{0\,c}$	1	0.26	0.12	0.19	140	30
	2	*d*	0.59			30
	3	0.85	0.74	0.80	110	30
	1	0.25	0.16	0.21	90	50
	2,3	0.80	0.72	0.76	80	50

[a] Potentials for first scan. [b] Potentials after several scans. [c] Potentials are given for second scan as initial oxidation response for process 3 merges with the background for first scan. [d] Oxidation response for process 2 is not clearly defined.

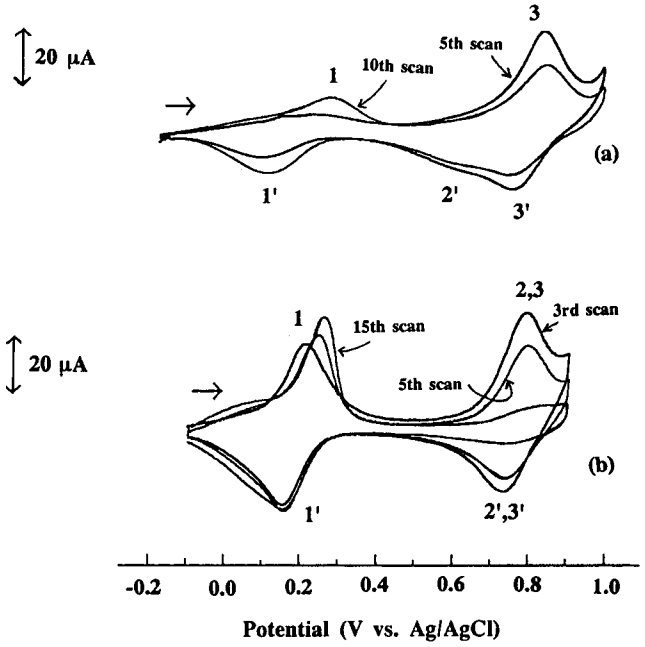

Figure 7. Cyclic voltammograms (scan rate, 200 mV s^{-1}) of solid *cis,mer*-$Mn(CO)_2(\eta^3\text{-}P_3P')Br$ mechanically attached to a graphite electrode and placed in aqueous solution (0.1 M NaCl) at (a) 30 and (b) 50 °C.

voltammograms at 50 °C in the solid state show characteristics similar to those in acetone solution at 20 °C.

(b) IR Spectroscopy and X-ray Electron Probe Analysis. Specular reflectance FT-IR spectroscopy confirms that *trans*-$[Mn(CO)_2(\eta^3\text{-}P_3P')Br]^+$ is generated by the oxidation of either solid *trans*- or *cis,mer*-$Mn(CO)_2(\eta^3\text{-}P_3P')Br$, and data are given in Table 2.

X-ray electron probe analysis of solid *trans*- or *cis,mer*-$Mn(CO)_2(\eta^3\text{-}P_3P')Br$ subsequent to oxidation at an electrode surface in contact with aqueous solution (0.1 M KCl) showed the presence of chloride (but not potassium), indicating that the anion enters the crystal lattice upon oxidation of each complex.

***trans*-[{$Mn(CO)_2(\eta^2$-dpe)Br}$_2(\mu$-dpe)]$(BF_4)_2$ *and cis,fac*-{$Mn(CO)_2(\eta^2$-dpe)Br}$_2(\mu$-dpe). (a) Electrochemical Studies.** The geometries of the compounds are given in structures **V** and **VI**. In dichloromethane

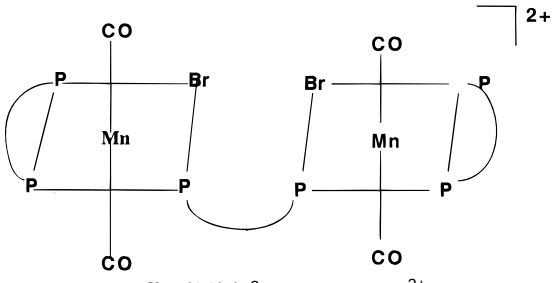

trans-[{$Mn(CO)_2(\eta^2$-dpe)Br}$_2(\mu$-dpe)]$^{2+}$ **(V)**

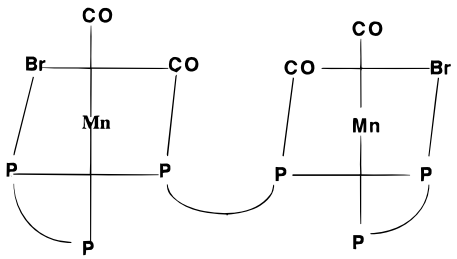

cis,fac-{$Mn(CO)_2(\eta^2$-dpe)Br}$_2(\mu$-dpe) **(VI)**

solution, *cis,fac*-{$Mn(CO)_2(\eta^2$-dpe)Br}$_2(\mu$-dpe) shows[7] two oxidation responses (designated processes 1 and 2) which are reversible at −50 °C, but at room temperature rapid (scan rate, 200 mV s^{-1}) isomerization occurs to give *trans* geometry at each manganese atom, so that processes 1 and 2 are irreversible. Two new reversible couples (3 and 4) are observed on the reverse and subsequent scans, due to the redox chemistry of the *trans*-$[\{Mn(CO)_2(\eta^2\text{-dpe})Br\}_2(\mu\text{-dpe})]^{2+/+/0}$ system, which does not isomerize back to *cis,mer* on the voltammetric time scale. These voltammetric reactions are summarized in eqs 5 and 6. Importantly, the successive

$$\textit{cis,fac}\text{-}\{Mn(CO)_2(\eta^2\text{-dpe})Br\}_2(\mu\text{-dpe}) \rightleftharpoons \textit{cis,fac}\text{-}[\{Mn(CO)_2(\eta^2\text{-dpe})Br\}_2(\mu\text{-dpe})]^+ + e^- \rightleftharpoons \textit{cis,fac}\text{-}[\{Mn(CO)_2(\eta^2\text{-dpe})Br\}_2(\mu\text{-dpe})]^{2+} + e^- \quad \text{(processes 1 and 2 at } -50\ ^\circ\text{C)} \quad (5)$$

$$\textit{trans}\text{-}\{Mn(CO)_2(\eta^2\text{-dpe})Br\}_2(\mu\text{-dpe}) \rightleftharpoons \textit{trans}\text{-}[\{Mn(CO)_2(\eta^2\text{-dpe})Br\}_2(\mu\text{-dpe})]^+ + e^- \rightleftharpoons \textit{trans}\text{-}[Mn(CO)_2(\eta^2\text{-dpe})Br\}_2(\mu\text{-dpe})]^{2+} + e^- \quad \text{(processes 3 and 4)} \quad (6)$$

oxidations and reductions occur in solution at considerably different potentials (approximately 120 mV) in both geometries, indicating that significant electronic communication occurs between the two metal centers in the one-electron oxidized species.

The first cycle of a reductive cyclic voltammogram at 20 °C (scan rate, 200 mV s^{-1}) of *trans*-[{$Mn(CO)_2(\eta^2$-

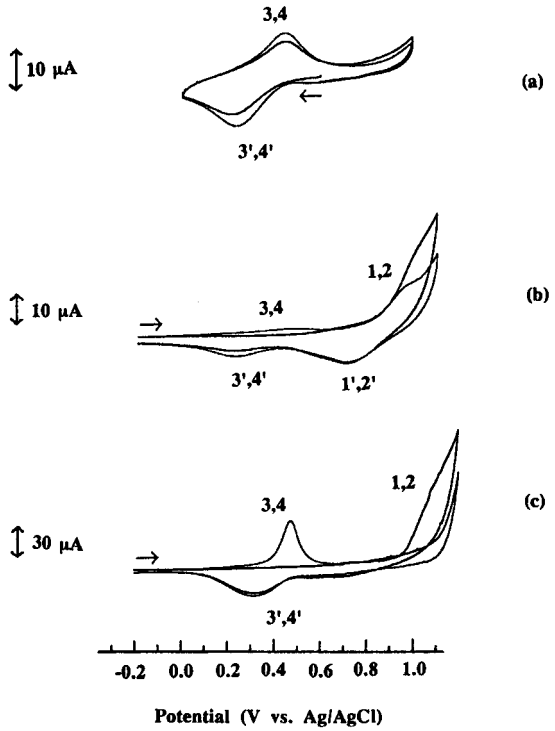

Figure 8. Cyclic voltammograms (scan rate, 200 mV s^{-1}) of solid complexes mechanically attached to graphite electrodes and placed in aqueous solution (0.1 M NaCl): (a) *trans*-[{$Mn(CO)_2(\eta^2$-dpe)$Br\}_2(\mu$-dpe)]BF_4 at 20 °C, (b) *cis,fac*-{$Mn(CO)_2(\eta^2$-dpe)$Br\}_2(\mu$-dpe) at 20 °C, and (c) *cis,fac*-{$Mn(CO)_2(\eta^2$-dpe)$Br\}_2(\mu$-dpe) at 50 °C.

dpe)$Br\}_2(\mu$-dpe)]$(BF_4)_2$ attached to a graphite electrode (Figure 8a) shows only a single reduction response at 0.22 V, and the corresponding single oxidation response is observed on the reverse scan at 0.45 V. Successive cycles show a small shift of the redox couple to a more positive potential, and the peak separation (ΔE_p) decreases on the second and subsequent cycles compared with the first cycle. Voltammograms at higher temperatures are similar, but at 40 and 50 °C the separations between oxidation and reduction peaks is smaller on the first cycle than on successive cycles, as detailed in Table 4. These data differ when compared to studies in dichloromethane solution,[7] where individual redox couples (processes 3 and 4) are observed for each metal center. The consecutive oxidations of the metal centers in the solution phase imply some electronic communication between metal centers, since these centers would be oxidized/reduced at the same potentials if this electronic interaction were absent. The solid state results suggest that electronic communication between the metals is not significant in the solid state and that the reversible couple observed is an overall two-electron process which generates *trans*-{$Mn(CO)_2(\eta^2$-dpe)$Br\}_2(\mu$-dpe) on the reduction scan. Since there are two electron steps, the designation 3,4 and 3′,4′ is used to define the processes for the binuclear species in the solid state. The voltammetric data do not reveal the role of the anions associated with the solid and with the electrolyte. However, data presented below reveal that an ion exchange process occurs, so the electrochemical reaction for *trans*-[{$Mn(CO)_2(\eta^2$-dpe)$Br\}_2(\mu$-dpe)]$^{2+}$ is as given in eqs 7a and 7b.

Electrochemical studies of solid *trans*-{$Mn(CO)_2(\eta^2$-dpe)$Br\}_2(\mu$-dpe) are not possible because this compound

Table 4. Voltammetric Data (Scan Rate, 200 mV s^{-1}) for Solid *trans*-[{$Mn(CO)_2(\eta^2$-dpe)$Br\}_2(\mu$-dpe)][BF_4]$_2$ and *cis,fac*-{$Mn(CO)_2(\eta^2$-dpe)$Br\}_2(\mu$-dpe) Mechanically Attached to Graphite Electrodes and Placed in Aqueous Solution (0.1 M NaCl)

		potential (V vs Ag/AgCl)				
compound	couple	E_p^{ox}	E_p^{red}	$E^r_{1/2}$	ΔE_p (mV)	temp (°C)
trans$^{+\,a}$	3,4	0.45	0.22	0.34	230	20
	3,4	0.46	0.24	0.35	220	30
	3,4	0.44	0.28	0.36	160	40
	3,4	0.47	0.33	0.40	140	50
trans$^{+\,b}$	3,4	0.44	0.25	0.35	190	20
	3,4	0.45	0.26	0.36	190	30
	3,4	0.44	0.26	0.35	180	40
	3,4	0.47	0.30	0.39	170	50
cis,fac$^{0\,c}$	1,2	0.98	0.71	0.85	270	20
	3,4	0.42	0.23	0.32	190	20
	3,4	0.47	0.33	0.40	140	50

[a] Potentials for first scan. [b] Potentials after several scans. [c] Potentials are given for second scan both at 20 °C as initial oxidation response for process 1 merges with the background for first scan and at 50 °C.

$$\textit{trans}\text{-}[\{Mn(CO)_2(\eta^2\text{-dpe})Br\}_2(\mu\text{-dpe})](BF_4)_{2\,s} + 2Cl^- \rightleftharpoons \textit{trans}\text{-}[\{Mn(CO)_2(\eta^2\text{-dpe})Br\}_2(\mu\text{-dpe})]Cl_{2\,s} + 2BF_4^- \quad (7a)$$

$$\textit{trans}\text{-}[\{Mn(CO)_2(\eta^2\text{-dpe})Br\}_2(\mu\text{-dpe})]Cl_{2\,s} + 2e^- \rightleftharpoons \textit{trans}\text{-}\{Mn(CO)_2(\eta^2\text{-dpe})Br\}_2(\mu\text{-dpe})_s + 2Cl^- \quad (7b)$$

has only been generated in solution at low temperature, with rapid isomerization to *cis,fac* geometry occurring at 20 °C.

A cyclic voltammogram (scan rate, 200 mV s^{-1}) recorded at 20 °C for the oxidation of solid *cis,fac*-{$Mn(CO)_2(\eta^2$-dpe)$Br\}_2(\mu$-dpe) attached to a graphite electrode is shown in Figure 8b. The first scan shows an oxidation response which merges with the solvent background, and the corresponding reduction wave is observed upon reversing the direction of the scan. A smaller reduction response also is apparent at a less positive potential, and this process is shown to be reversible when a second cycle is recorded. The second scan shows a more defined oxidation response for the reversible couple at 0.85 V than that observed on the first scan, and the current associated with the redox couple at the lower potential increases on further cycling of the potential. Voltammograms of *cis,fac*-{$Mn(CO)_2$-(η^2-dpe)$Br\}_2(\mu$-dpe) in dichloromethane solution at 20 °C show[7] two irreversible oxidation responses (processes 1 and 2), which are associated with consecutive oxidations of the metal centers, followed in each case by rapid isomerization to *trans* geometry. However, at lower temperatures these solution phase responses become reversible, due to a decrease in the isomerization rate constants. The observation of a reversible response ($E^r_{1/2}$ = 0.85 V) at 20 °C in the solid state gives further evidence for a decrease in the rate constants for isomerizations involving surface-attached species. Since process 3,4 is observed on repetitive cycling, the reversible couple at $E^r_{1/2}$ = 0.85 V is assigned to both processes 1 and 2, since only a single redox couple is apparent for solid *trans*-[{$Mn(CO)_2(\eta^2$-dpe)$Br\}_2(\mu$-dpe)]$(BF_4)_2$, in contrast to electrochemical studies in dichloromethane solution. The reaction in the solid state is summarized

by the mechanism

$$\begin{aligned} &cis,fac\text{-}\{Mn(CO)_2(\eta^2\text{-dpe})Br\}_2(\mu\text{-dpe})_s + 2Cl^- \\ &\rightleftharpoons cis,fac\text{-}[\{Mn(CO)_2(\eta^2\text{-dpe})Br\}_2(\mu\text{-dpe})]Cl_{2\ s} + 2e^- \\ &\xrightarrow{\text{very slow}} trans\text{-}[\{Mn(CO)_2(\eta^2\text{-dpe})Br\}_2(\mu\text{-dpe})]Cl_{2\ s} \\ &+ 2e^- \rightleftharpoons trans\text{-}\{Mn(CO)_2(\eta^2\text{-dpe})Br\}_2(\mu\text{-dpe})_s + 2Cl^- \end{aligned} \quad (8)$$

Figure 8c shows a series of cyclic voltammograms (scan rate, 200 mV s^{-1}) for the oxidation of solid *cis,fac*-$\{Mn(CO)_2(\eta^2\text{-dpe})Br\}_2(\mu\text{-dpe})$ at 50 °C. On the first cycle, an irreversible oxidation response corresponding to process 1,2 is barely detected above the solvent background, while the reverse scan shows a very well-defined single reduction wave due to process 3′,4′. A second cycle reveals the oxidation response attributed to process 3,4, but, unlike the case at 20 °C, no oxidative current is observed for process 1,2 on the second scan. Thus, the oxidation of *cis,fac*-$\{Mn(CO)_2(\eta^2\text{-dpe})Br\}_2(\mu\text{-dpe})$ generates *cis,fac*-$[\{Mn(CO)_2(\eta^2\text{-dpe})Br\}_2(\mu\text{-dpe})]^{2+}$, which isomerizes to *trans*-$[\{Mn(CO)_2(\eta^2\text{-dpe})Br\}_2(\mu\text{-dpe})]^{2+}$, and, as expected, this isomerization is faster at 50 than at 20 °C.

(b) IR Spectroscopy and X-ray Electron Probe Analysis. Specular reflectance FT-IR spectroscopy shows that the two carbonyl bands of solid *cis,fac*-$\{Mn(CO)_2(\eta^2\text{-dpe})Br\}_2(\mu\text{-dpe})$ attached to a graphite electrode disappear upon oxidation of this complex and are replaced by the single carbonyl stretch of *trans*-$[\{Mn(CO)_2(\eta^2\text{-dpe})Br\}_2(\mu\text{-dpe})]^{2+}$. This experiment confirms that the oxidation process is a two-electron process. IR data are summarized in Table 2.

X-ray electron probe microanalysis indicates the presence of chloride subsequent to oxidation of *cis,fac*-$\{Mn(CO)_2(\eta^2\text{-dpe})Br\}_2(\mu\text{-dpe})$ at the solid−electrode−water (0.1 M KCl) interface. In experiments involving *trans*-$[\{Mn(CO)_2(\eta^2\text{-dpe})Br\}_2(\mu\text{-dpe})](BF_4)_2$, which was first reduced at 0.100 V and then reoxidized at 0.600 V, the technique indicates that Cl^- replaces BF_4^- in the solid.

Conclusions

Electrochemical oxidation of solid *cis,mer*-$Mn(CO)_2(\eta^3\text{-}P_2P')Br$ at a graphite electrode−water (electrolyte) interface leads to the observation of the three redox couples (*cis,mer*$^{+/0}$, *cis,fac*$^{+/0}$, and *trans*$^{+/0}$), with the 17-electron *trans*$^+$ species being the thermodynamically stable geometry in the oxidized form in the solid state. Likewise, oxidative studies of solid *cis,mer*-$Mn(CO)_2(\eta^3\text{-}P_3P')Br$ indicated isomerization of the 17-electron *cis,mer*$^+$ to the *cis,fac*$^+$ and *trans*$^+$ geometries. The faster isomerization reaction in solution between the *cis,mer*$^+$ and *cis,fac*$^+$ isomers of the P_3P' complexes, compared with that of the analogous P_2P' complexes (due to steric effects), also applies in the solid state. As expected, the rates of isomerization increased upon increasing the temperature, but a decrease in the rate constants for the isomerization reactions was noted for the surface-attached species relative to values in solution. The slower rate for the studies on solids also was apparent for oxidative studies of the binuclear complex *cis,fac*-$\{Mn(CO)_2(\eta^2\text{-dpe})Br\}_2(\mu\text{-dpe})$, for which a single reversible two-electron oxidation response was observed at 20 °C, in contrast to the two irreversible oxidation waves in dichloromethane solution at 20 °C. The presence of one two-electron responses, rather than two well-separated one-electron responses, was attributed to a decrease in communication between the metal centers in the solid state, presumably related to decreased flexibility of the complexes in the solid state.

Monitoring of the surface-confined redox processes by specular reflectance FT-IR spectroscopy verifies that, in each case, the 18-electron *cis* or *trans* complexes are oxidized to the 17-electron *trans*$^+$ species. This oxidation process is accompanied by the uptake of chloride ions from the supporting electrolyte into the solid, as shown by X-ray electron probe microanalysis. The incorporation of chloride was noted also for the experiments where the *trans*$^+$ tetrafluoroborate species attached to the electrode is first reduced at a fixed potential (and, thus, BF_4^- is expelled from the solid) and then reoxidized.

Acknowledgment. We thank the Australian Research Council for financial support. J.N.W. thanks the Commonwealth Government of Australia for a Post Graduate Research Award.

OM970468J